

Investigation of doublet-bands in $^{124,126,130,132}\text{Cs}$ odd-odd nuclei using triaxial projected shell model approach

G.H. Bhat¹, R.N. Ali¹, J.A. Sheikh^{1,2} and R. Palit³

¹*Department of Physics, University of Kashmir, Srinagar, 190 006, India*

²*Department of Physics and Astronomy, University of Tennessee, Knoxville, TN 37996, USA*

³*Department of Nuclear and Atomic Physics, Tata Institute of Fundamental Research, Colaba, Mumbai, 400 005, India*

Abstract

Doublet bands observed in $^{124,126,130,132}\text{Cs}$ isotopes are studied using the recently developed multi-quasiparticle microscopic triaxial projected shell model (TPSM) approach. It is shown that TPSM results for energies and transition probabilities are in good agreement with known energies and the recently measured extensive data on transition probabilities for the bands in ^{126}Cs . In particular, it is demonstrated that characteristic transition probabilities expected for the doublet bands to originate from the chiral symmetry breaking are well reproduced in the present work. The calculated energies for $^{124,130,132}\text{Cs}$ are also shown to be in reasonable agreement with the available experimental data. Furthermore, a complete set of the calculated transition probabilities is provided for the doublet bands in $^{124,130,132}\text{Cs}$ isotopes.

Key words: triaxial deformation, γ -vibration, two-quasiparticle states, triaxial projected shell model

PACS: 21.60.Cs, 21.10.Hw, 21.10.Ky, 27.50.+e

1 Introduction

The observation of chiral rotation in atomic nuclei has attracted a considerable attention in recent years. It has been demonstrated that band structures of triaxial odd-odd nuclei in $A \sim 100$ and ~ 130 regions show characteristic properties of chiral symmetry breaking in the intrinsic frame [1,2,3,4]. In the $A \sim 130$ region, odd-proton (odd-neutron) occupies lower-half (upper-half) of the intruder sub-shell $1h_{11/2}$ with their angular-momentum vectors

aligned toward short (long) principal-axis of the triaxial density distribution. The core angular-momentum vector, on the other hand, is directed along the intermediate axis as it has the largest irrotational moment of inertia. The three orthogonal angular-momentum vectors of odd-proton, odd-neutron and the core give rise to chiral geometry [5]. The manifestation of the chiral geometry in the laboratory frame is the appearance of $\Delta I = 1$ doublet band structures with similar γ -ray energies [6,7]. Although, near degenerate doublet bands have been observed in many odd-odd nuclei as well as in odd-mass nuclei, however, it is now well recognised that several of these bands don't originate from the chiral symmetry breaking [8,9,10,11,12,13]. The stringent selection rules imposed by chiral symmetry on the wavefunction in the form of characteristic transition probabilities are not obeyed by many nuclei, although, they depict near degenerate doublet bands[14,15]. The measurement of transition probabilities, therefore, plays a very critical role in the establishment of chiral geometry for a given system. Previously, ^{128}Cs was the best known example where most of the selection rules on γ -transitions governed by spontaneous chiral symmetry breaking were approximately satisfied [16]. For this nucleus, the energy separation between the doublet bands is approximately 200 keV and the energy staggering is very small. $B(E2)(I \rightarrow I - 2)$ transitions were measured up to spin, $I = 20$ for the yrast and up to $I = 17$ for the side band. These $B(E2)$ values for the two bands are quite similar, which confirms that doublet bands originate from the same intrinsic configuration. $B(M1)(I \rightarrow I - 1)$ transitions for yrast \rightarrow yrast, side \rightarrow side and side \rightarrow yrast were measured up to spins of $I = 18, 17$ and 16 , respectively. It is evident from the data that $B(M1)$ transitions for side \rightarrow yrast have staggering phase opposite to that of yrast \rightarrow yrast and side \rightarrow side phase, which is a result of the selection rule originating from the chiral symmetry. These observed properties of the chiral bands in ^{128}Cs have been studied using the triaxial particle-rotor model [16] and also were investigated recently using the triaxial projected Shell model (TPSM) approach [17]. It was demonstrated that TPSM gives a slightly better description of the observed data as compared to the particle-rotor model approach. In particular, it was shown that TPSM correctly reproduces the observed trend in the measured $B(E2)$ transitions as a function of spin.

The purpose of the present work is to perform a systematic investigation of the observed doublet band structures in odd-odd Cs-isotopes using the TPSM approach. Recently, using the doppler shift attenuation (DSA) method, 13 lifetimes and 26 corresponding absolute transition probabilities were obtained for ^{126}Cs [18]. This set of data on transition probabilities is more exhaustive than that of ^{128}Cs and it is possible to test the spontaneous breaking of chiral symmetry more completely. For other Cs-isotopes, studied in the present work, limited data for the doublet-bands is available for the transition energies only and we provide a complete set of transition probabilities for these nuclei using the TPSM approach to be compared with the future experimental

measurements.

The present manuscript is organized as follows. In section II, we shall present a few elements of the TPSM approach that are relevant in the discussion of the results. The details of the TPSM approach have already been presented in our earlier publications, for instance, in ref. [17]. The obtained results are displayed and discussed in section III and finally summary and conclusions are provided in section IV.

2 Triaxial projected shell model approach

For odd-odd nuclei, the TPSM basis space consists of one-neutron plus one-proton quasiparticle configurations [19,20] :

$$\{|\phi_\kappa\rangle = a_\nu^\dagger a_\pi^\dagger |0\rangle\}. \quad (1)$$

As almost all the doublet bands observed in odd-odd nuclei are built on one-neutron plus one-proton configurations, the above chosen basis is adequate to discuss the doublet band structures. In Eq. (1), $|0\rangle$ is the quasiparticle vacuum state and is obtained through diagonalization of the deformed Nilsson Hamiltonian with a subsequent BCS calculations. The number of basis configurations in Eq. (1) depend on the number of levels near the respective Fermi levels of protons and neutrons.

It should be noted that the states $|\phi_\kappa\rangle$ constructed from the diagonalization of the deformed Nilsson Hamiltonian do not conserve rotational symmetry. In order to restore this symmetry, three-dimensional angular-momentum projection technique is applied [21]. From each intrinsic state, κ , in (1) a band is generated through projection technique. The interaction between different bands for a given spin is taken into account by diagonalizing the shell model Hamiltonian in the projected basis. The Hamiltonian employed in the present work is given by

$$\hat{H} = \hat{H}_0 - \frac{1}{2}\chi \sum_\mu \hat{Q}_\mu^\dagger \hat{Q}_\mu - G_M \hat{P}^\dagger \hat{P} - G_Q \sum_\mu \hat{P}_\mu^\dagger \hat{P}_\mu, \quad (2)$$

and the corresponding triaxial Nilsson Hamiltonian is given by

$$\hat{H}_N = \hat{H}_0 - \frac{2}{3}\hbar\omega \left\{ \epsilon \hat{Q}_0 + \epsilon' \frac{\hat{Q}_{+2} + \hat{Q}_{-2}}{\sqrt{2}} \right\}, \quad (3)$$

Table 1

Axial deformation parameter (ϵ) and triaxial deformation parameter (ϵ') employed in the calculation for $^{124,126,130,132}\text{Cs}$ -isotopes.

	^{124}Cs	^{126}Cs	^{130}Cs	^{132}Cs
ϵ	0.256	0.260	0.160	0.170
ϵ'	0.170	0.150	0.145	0.150

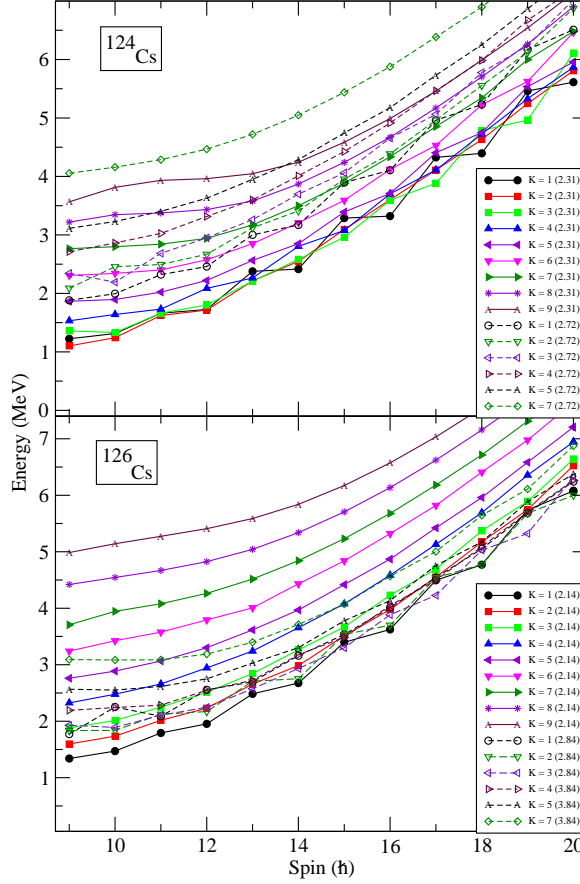


Fig. 1. (Color online) Angular-momentum projected bands obtained for different intrinsic K-configuration, given in the legend box, for $^{124,126}\text{Cs}$ nuclei. The energies of the triaxial quasiparticle states are given in the parenthesis.

where \hat{H}_0 is the spherical single-particle shell model Hamiltonian, which contains the spin-orbit force [22]. The second, third and fourth terms in Eq. (2) represent quadrupole-quadrupole, monopole-pairing, and quadrupole-pairing interactions, respectively. The axial and triaxial terms of the Nilsson potential in Eq. 3 contain the parameters ϵ and ϵ' , respectively, which are approximately related to the γ -deformation parameter by $\gamma = \tan^{-1}(\frac{\epsilon'}{\epsilon})$. The strength of the quadrupole-quadrupole force χ is determined in such a way that the employed quadrupole deformation ϵ is same as obtained by the Hartree-Fock-Bogoliubov (HFB) procedure. The monopole-pairing force constants G_M used in the cal-

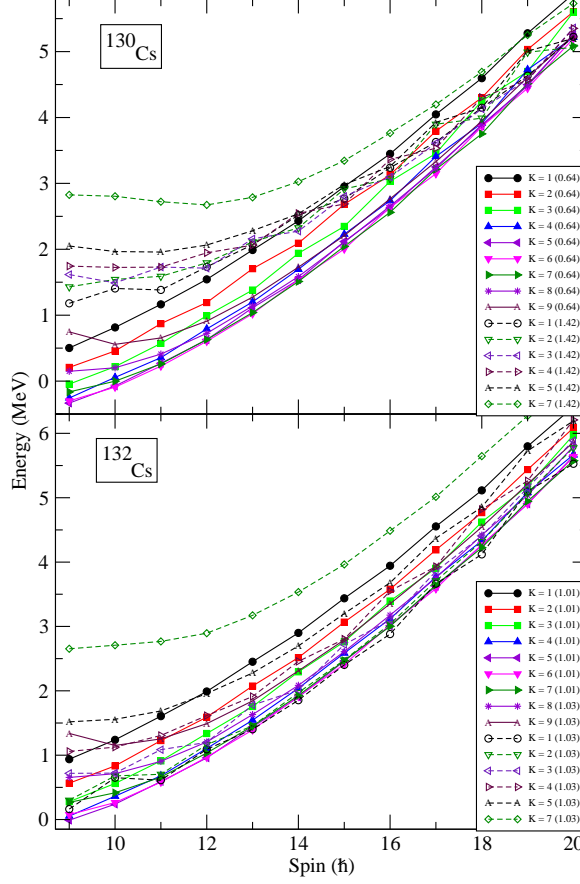


Fig. 2. (Color online) The angular-momentum projected bands obtained for different intrinsic K-configuration, given in legend box, for $^{130,132}\text{Cs}$ nuclei. The energies of the triaxial quasiparticle states are given in the parenthesis.

culations are

$$G_M^\nu = [20.12 - 13.13 \frac{N - Z}{A}] A^{-1}, \quad G_M^\pi = 20.12 A^{-1}. \quad (4)$$

The quadrupole pairing strength G_Q is assumed to be proportional to the monopole strength, $G_Q = 0.16 G_M$. All these interaction strengths are the same as those used in our earlier studies [17,19,20].

3 Results and discussions

The investigation of the properties of a triaxial system using the TPSM approach proceeds in several stages. In the first stage, the triaxial intrinsic states are constructed by solving the three-dimensional Nilsson potential with input axial and non-axial deformation parameters. The deformations employed for the Cs-isotopes investigated in the present work are listed in Table I.

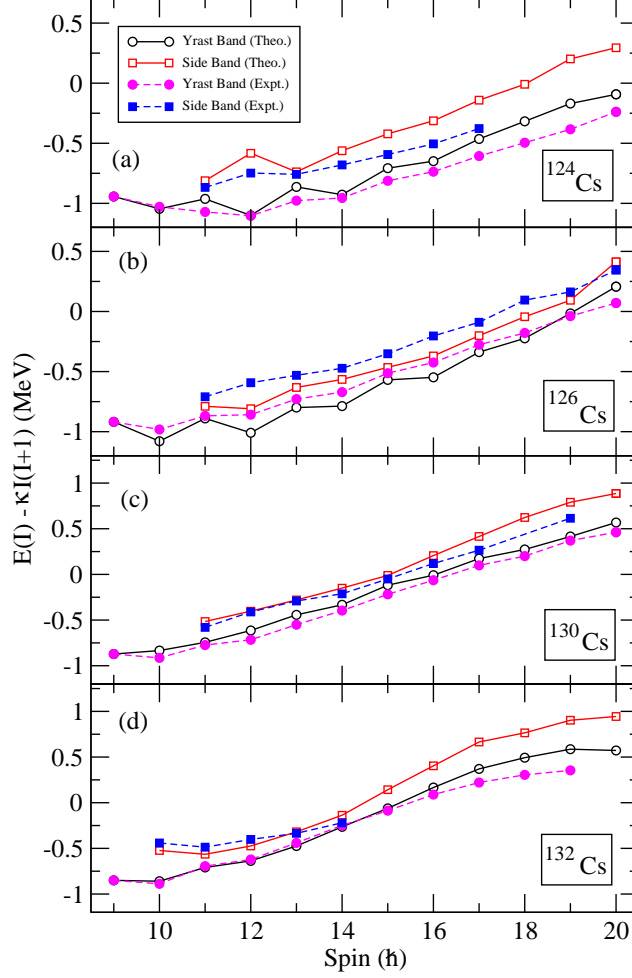


Fig. 3. (Color online) Comparison of the TPSM energies, after configuration mixing with the available experimental data for the yrast and side bands of the studied $^{124,126,130,132}\text{Cs}$ nuclei. The value of κ , shown in y-axis, is defined as $\kappa = 32.32A^{-5/3}$. Data have been taken from Refs. [18,23,27,32]

The axial deformation values have been adopted from the earlier studies [8,23,24,25,26,27] and the chosen value of non-axial deformation approximately corresponds to $\gamma \sim 30^\circ$.

In the second stage, three-dimensional angular-momentum projection technique is used to project the intrinsic triaxial basis onto good angular-momentum states. The lowest projected bands obtained for the studied ^{124}Cs , ^{126}Cs , ^{130}Cs and ^{132}Cs nuclei are shown in Figs. 1 and 2. The projected bands displayed in the two figures are referred to as the band diagrams and are quite instructive to unravel the intrinsic quasiparticle structures of the observed bands. For ^{124}Cs , it is evident from the top panel of Fig. 1 that many configurations contribute for the yrast spectroscopy for all the studied spin values. For low-spin values, $K=1,2$ and 3 projected bands from the two-quasiparticle configuration with energy 2.31 MeV are almost degenerate. For high-spin states, $K=4$ and

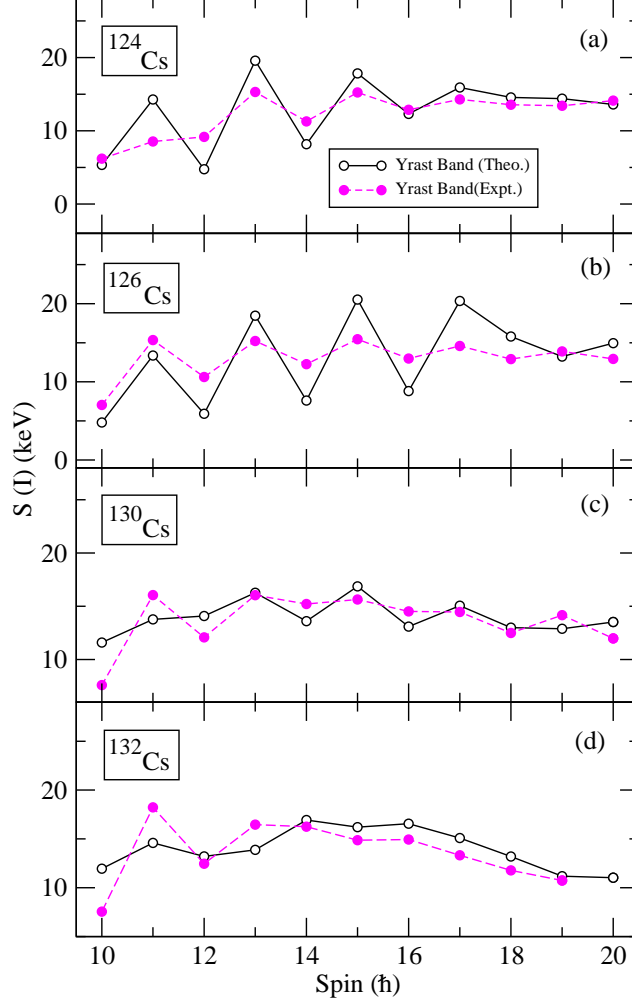


Fig. 4. (Color online) Calculated staggering parameter $S(I) = [E(I) - E(I - 1)] / 2I$ is plotted along with the measured values in panels.

5 bands also become favourable and the strong odd-even staggering in the $K=1$ band leads odd-spin members of the lowest band resulting from the $K=3$ configuration. The projected bands from the other quasiparticle state with energy equal to 2.72 MeV lie at higher excitation energies and don't become favourable for the studied spin values. The band diagram for ^{126}Cs , shown in the bottom panel of Fig. 1, has lowest two bands having $K=1$ and 2 in the low-spin regime, originating from the same intrinsic quasiparticle state. For higher-spins, it is noted that several bands contribute to the near yrast spectroscopy. Further, due to odd-even staggering in the $K=1$ band, the lowest odd-spin member at high-spin has $K=3$ and originate from a different quasiparticle state in comparison to the even-spin. As will be demonstrated later, these structural changes at high-spins are reflected in the observed transition probabilities.

The band diagram for ^{130}Cs , shown in the upper panel of Fig. 2, depicts

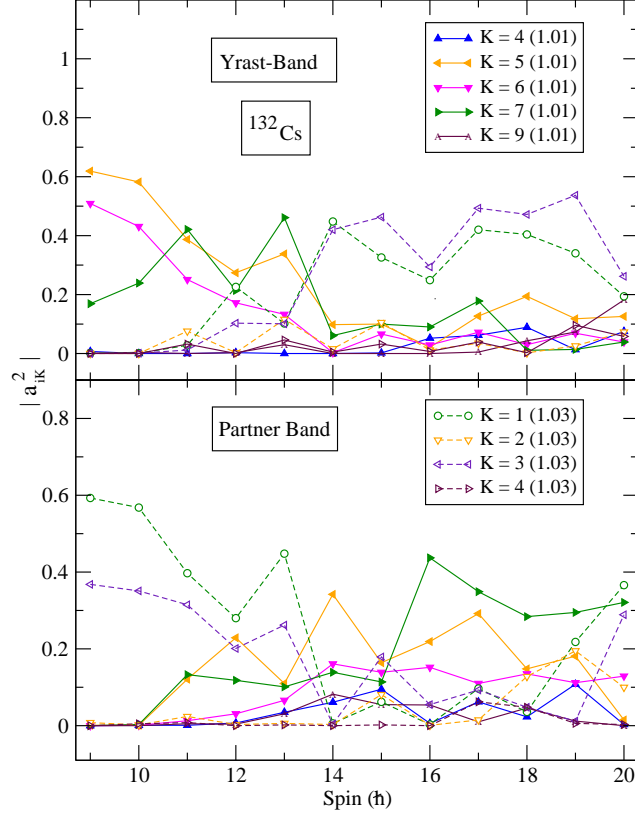


Fig. 5. (Color online) Probability of various projected K-configurations in the wavefunctions of the yrast and the first excited bands for ^{132}Cs

K=4,5,6 and 7 configurations, projected from the quasiparticle state with energy 0.64 MeV, dominating the yrast spectroscopy over the whole studied spin regime. However, it is noted that above I=19, the projected configurations from the quasiparticle state with energy equal to 1.42 MeV are beginning to play important role for the yrast states. The band diagram for ^{132}Cs displays quite an interesting projected band structures. For low-spin states, the yrast band is dominated by K=4,5,6 and 7 projected from the quasiparticle state with energy equal to 1.01 MeV, however, at I=14, it is seen that projected K=1 band from the quasiparticle state with energy equal to 1.03 MeV crosses and becomes yrast. This crossing is quite interesting as the partner band in ^{132}Cs is observed, to be discussed later, only up to I=14.

In the third and final stage, the projected basis, obtained above, are then employed for diagonalisation of the shell model Hamiltonian, Eq. (2). The energies obtained, after diagonalisation, for the lowest two bands are depicted in Fig. 3 for the four studied isotopes. The excitation energies have been subtracted by the core contribution in order to highlight the differences. It is evident from the figure that the agreement between the calculated and the measured energies is quite satisfactory. The odd-even staggering observed for the yrast-band at lower-spin values in $^{124-126}\text{Cs}$ isotopes is well reproduced

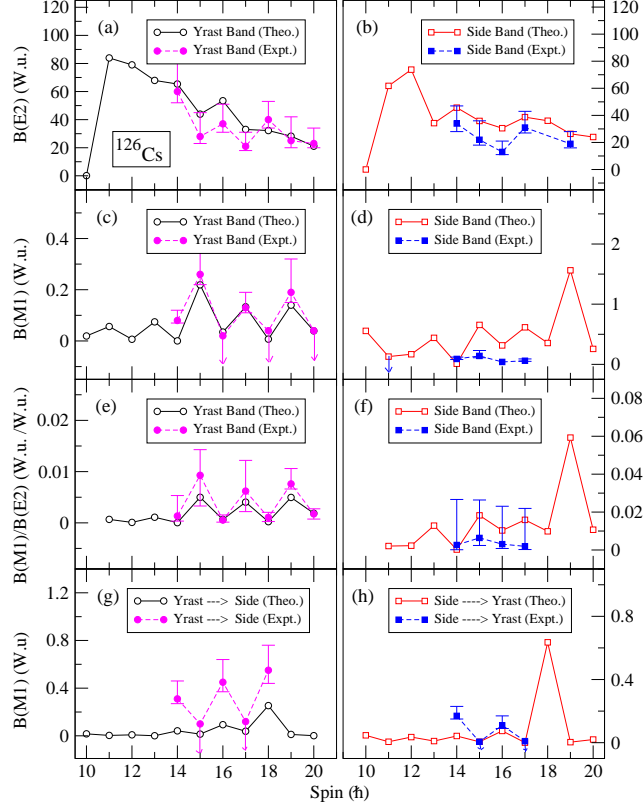


Fig. 6. (Color online) Comparison of the experimental $B(E2)$, $B(M1)$ transition strengths and their ratios for ^{126}Cs [18] with the calculated values for yrast and side bands are depicted in panels (a) to (f). The calculated inter-band transitions are shown in panels (g) and (h), and these panels also depicts the measured values for a few transitions.

by the TPSM calculations. For a better visualisation of the odd-even effect, the staggering parameter, $S(I) = [E(I) - E(I - 1)]/2I$ is plotted in Fig. 4 for the yrast-bands of the four studied nuclei. For the low-spin values, the calculated staggering is larger than the observed and this discrepancy seems to be inherent in most of the earlier theoretical investigations [26,27,28,29].

It is interesting to note from Fig. 3 that in ^{132}Cs , yrast and the first-excited bands become almost degenerate at $I=14$ and the observed partner band is known only up to this spin value. The reason for this degeneracy can be traced to the crossing of the projected bands originating from two different quasiparticle configurations in Fig. 1 at this spin value. To investigate the nature of the doublet-bands in ^{132}Cs after diagonalisation, the probability of various projected configurations in the two wavefunctions are displayed in Fig. 5. For the yrast band, the dominant configurations up to $I=13$ are $K=5,6$ and 7 from the quasiparticle state with energy 1.01 MeV. Above $I=13$, the yrast band is composed of the projected configurations, originating from the quasiparticle state with energy 1.03 MeV. For the partner-band, the structure is quite opposite to that of the yrast-band with 1.03 MeV quasiparticle state

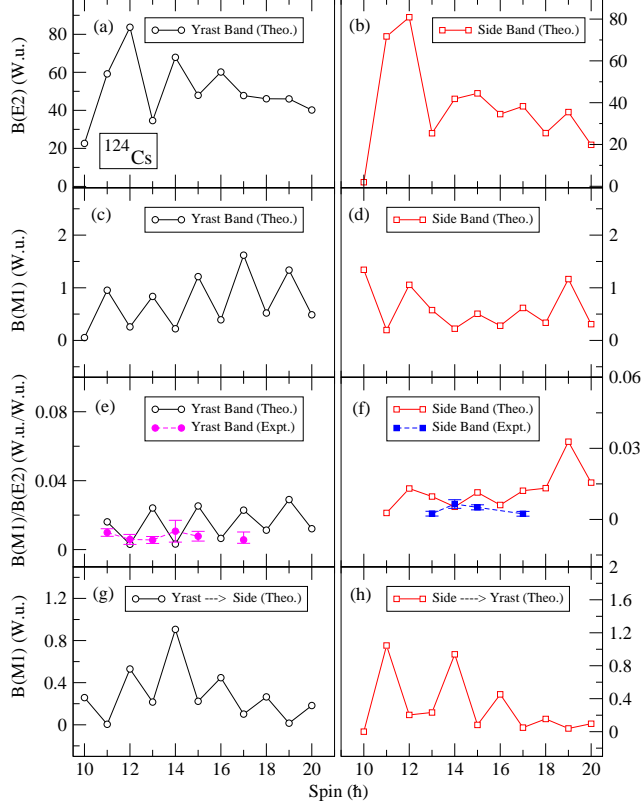


Fig. 7. (Color online) The calculated $B(E2)$, $B(M1)$ transition strengths and their ratios for ^{124}Cs are depicted in panels (a) to (f). The measured ratios [23] are also shown in the panels (e) and (f) The calculated inter-band transitions are shown in panels (g) and (h).

dominating up to $I=13$ and above this spin value, it is the other quasiparticle state becoming important. Therefore, it is predicted in the present work that the yrast and the partner bands change their character at $I=14$.

We shall now turn to the discussion of the electromagnetic transition probabilities, which play a crucial role to determine whether the doublet bands originate from the breaking of the chiral symmetry. The transition probabilities have been evaluated using the expressions provided in our recent work [17] with the parameters : $g_l^\pi = 1$, $g_l^\nu = 0$, $g_s^\pi = 5.586 \times 0.85$, $g_s^\nu = -3.826 \times 0.85$, and the effective charges of $e^\pi = 1.5e$ and $e^\nu = 0.5e$. The transition probabilities are depicted in Figs. 6, 7, 8 and 9 for ^{126}Cs , ^{124}Cs , ^{130}Cs and ^{132}Cs , respectively. It is seen from Fig. 6 that both the behaviour and the magnitudes of the observed transitions for ^{126}Cs are reproduced reasonably well by the TPSM approach. In particular, the observed drop in the $B(E2)$ transitions with spin, Fig. 6(a), is correctly reproduced. To reproduce this behaviour in the $B(E2)$ transitions, also observed in ^{128}Cs , has been a drawback of the particle-rotor model description for these nuclei [16]. The staggering of the $B(E2)$ transitions in the spin regime between $I=14$ and 18 can be traced to the interplay between $K=1$ and 3 quasiparticle configurations as is evident

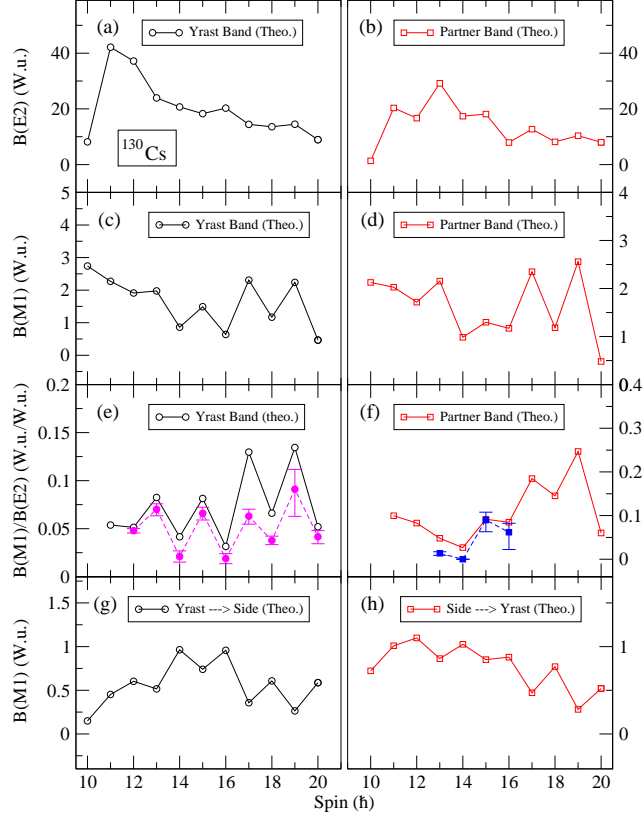


Fig. 8. (Color online) The calculated $B(E2)$, $B(M1)$ transition strengths and their ratios for ^{130}Cs are depicted in panels (a) to (f). The measured ratios [32] are also shown in the panels (e) and (f). The calculated inter-band transitions are shown in panels (g) and (h).

from the band diagram of Fig. 1. The wavefunctions after diagonalization, although, are highly mixed, but it is clearly noted that even- and odd-spin members of the yrast-band have different K -decompositions.

It has been already mentioned that chiral geometry imposes stringent selection rules [30] on the wavefunction with the resulting characteristic transition probabilities. For chiral geometry, $B(M1)$ transitions are expected to depict odd-even staggering with the phase of the in-band transitions opposite to that of inter-band transitions for the two chiral bands. This behaviour of the $B(M1)$ transitions is evident from Fig. 6 (c), (d), (g) and (h) in both observed as well as in the TPSM results. Some discrepancies between the TPSM results and the experimental values are noted in Figs. 6(d) and (g) for the side- and the yrast-to-side band $B(M1)$ transitions.

The calculated transition probabilities for ^{124}Cs , shown in Fig. 7, depict similar behaviour as that of ^{126}Cs . However, as compared to ^{126}Cs , $B(E2)$ depict odd-even staggering even for low-spin values and the reason for this can be traced to the interplay among several configurations in the low-spin regime as is evident from the band diagram plot of Fig. 1. The odd-even staggering in the $B(M1)$

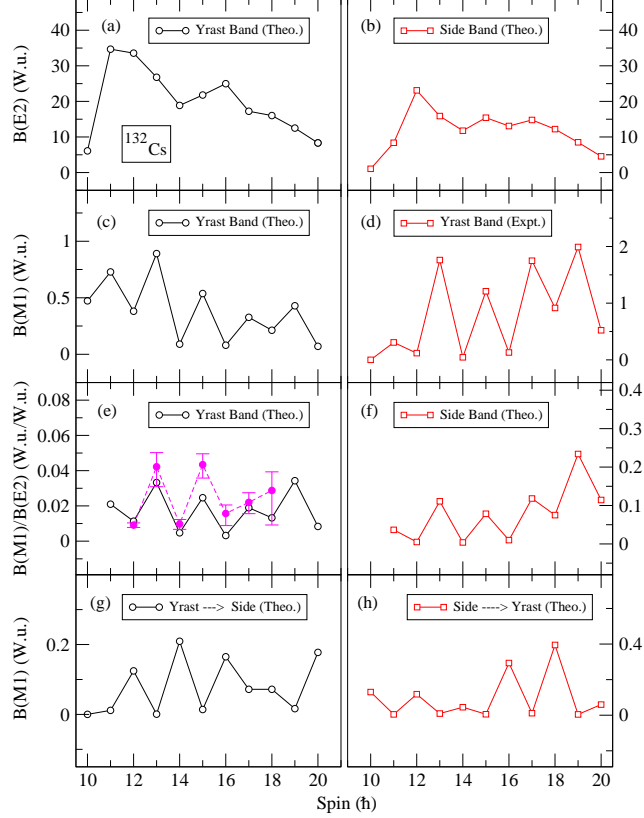


Fig. 9. (Color online) The calculated $B(E2)$, $B(M1)$ transition strengths and their ratios for ^{132}Cs are depicted in panels (a) to (f). The measured ratios [27] are also shown in the panels (e) and (f). The calculated inter-band transitions are shown in panels (g) and (h).

for this system is smaller than that of ^{126}Cs , but has the characteristic feature of the chiral geometry with the phase of in-band transitions opposite to that of inter-band transitions. Transition probabilities have not been measured for this system and only the ratios of $B(M1)/B(E2)$, calculated from the intensities, are depicted in Fig. 7.

The transition probabilities for ^{130}Cs , displayed in Fig. 8, show $B(E2)$ dropping with spin for the yrast configuration and for the partner band $B(E2)$ depict odd-even staggering since it is composed of low- K projected states. $B(M1)$ transitions in Fig. 8 have features as those expected for chiral bands. For ^{132}Cs , electromagnetic transitions are depicted in Fig. 9 with $B(E2)$ for the yrast band dropping with spin as for the other studied isotopes. The only difference is that above $I=13$, $B(E2)$'s depict odd-even staggering and is due to dominance of the $K=1$ projected state above $I=13$. $B(M1)$ transitions in Fig. 9 again have the behaviour as those expected for the chiral bands. The variation of the measured $B(M1)/B(E2)$ ratios for the yrast band with spin in ^{130}Cs and ^{132}Cs are well reproduced in the present calculations as shown in Fig. 8(e) and Fig. 9(e), respectively. Similarly, for the partner band of ^{130}Cs ,

the calculated $B(M1)/B(E2)$ ratios are in agreement with the measured values (see Fig. 8(f)).

4 Summary and conclusions

In the present work a systematic investigation of the doublet-bands observed in the four Cs-isotopes with mass numbers of 124,126,130 and 132 has been performed using the recently developed multi-quasiparticle TPSM approach. The transition energies of the doublet-bands are known for all the four isotopes up to high-spin and depict similar γ -ray energies and have been proposed to originate from the chiral symmetry breaking. However, it has been demonstrated [14] that the near degeneracy of the observed doublet-bands don't necessarily imply that the bands originate from the breaking of the chiral symmetry. The important clues on the nature of the doublet-bands is contained in the electromagnetic transition probabilities. It has been shown in a model study [31] that for doublet-bands to originate from the breaking of the chiral symmetry, the transitions probabilities must obey very special selection rules. For chiral bands, it is expected that $B(M1)$ transitions depict staggering with in-band transition showing opposite phase to that inter-band transitions. Although, these selection rules have been established in a simplified model, nevertheless, it is expected these should be obeyed approximately in realistic models.

Recently, a detailed experimental study on the electromagnetic transitions [18] has been performed for the doublet-bands observed in ^{126}Cs and this data is more exhaustive than the previously best studied ^{128}Cs system. It has been shown that TPSM approach provides a consistent description of the energies and the measured transition probabilities for ^{126}Cs . Further, it has been demonstrated that results are consistent with the chiral interpretation for the observed doublet bands. The predicted transition probabilities for $^{124,130,132}\text{Cs}$ isotopes also depict characteristic features of chiral symmetry breaking for the observed bands and it is highly desirable to perform lifetime measurements for the observed doublet-bands in order to confirm the chiral interpretation for these systems.

References

- [1] V.I. Dimitrov, S. Frauendorf, F. Donau, Phys. Rev. Lett. **84** (2000) 5732.
- [2] K. Starosta *et. al.*, Phys. Rev. C **65** (2002) 044328.
- [3] P. Olbratowski, J. Dobazewski, J. Dudek, W. Plöciennik, Phys. Rev. Lett. **93** (2004) 052501.

- [4] C. Vaman, D.B. Fossan, T. Koike, K. Starosta, I.Y. Lee, A.O. Macchiavelli, Phys. Rev. Lett. **92** (2001) 032501.
- [5] S. Frauendorf and J. Meng, Nucl. Phys. A **617** (1997) 131.
- [6] K. Starosta, T. Koike, C.J. Chiara, D.B. Fossan, D.R. Lafosse, Nucl. Phys. A **682** (2001) 375.
- [7] T. Koike, K. Starosta, C.J. Chiara, D.B. Fossan, D.R. LaFosse, Phys. Rev. C **67** (2003) 044319.
- [8] K. Starosta *et. al.*, Phys. Rev. Lett. **86** (2001) 971.
- [9] A.A. Hecht *et. al.*, Phys. Rev. C **63** (2001) 051302.
- [10] S. Zhu *et. al.*, Phys. Rev. Lett. **91** (2003) 132501.
- [11] V.I. Dimitrov, S. Frauendorf, F. Dönau, Phys. Rev. Lett. **84** (2000) 5732.
- [12] S.Q. Zhang, B. Qi, S.Y. Wang, J. Meng, Phys. Rev. C **75** (2007) 044307.
- [13] D. Tonev *et. al.*, Phys. Rev. Lett. **96** (2006) 052501.
- [14] C.M. Petrache, G.B. Hagemann, I. Hamamoto, K. Starosta, Phys. Rev. Lett. **96** (2006) 112502.
- [15] D.Tonev *et. al.*, Phys. Rev. C **76** (2007) 044313.
- [16] E. Grodner *et. al.*, Phys. Rev. Lett. **97** (2006) 172501.
- [17] G.H. Bhat, J.A. Sheikh, R. Palit, Phys. Lett. B **707** (2012) 250.
- [18] E. Grodner *et. al.*, Phys. Lett. B **703** (2011) 46.
- [19] R. Palit, J.A. Sheikh, Y. Sun, H.C. Jain, Phys. Rev. C **67** (2001) 014321.
- [20] R. Palit, J.A. Sheikh, Y. Sun, H.C. Jain, Nucl. Phys. A **686** (2001) 141.
- [21] P. Ring and P. Schuck, *The Nuclear Many-Body Problem* (Springer, New York, 1980).
- [22] S.G. Nilsson *et. al.*, Nucl. Phys. A **131** (1969) 1.
- [23] A. Gizon *et. al.*, Nucl. Phys. A **694** (2001) 63.
- [24] S.Y. Wang, B. Qi, D.P. Sun, Phys. Rev. C **82** (2010) 027303.
- [25] J. Meng, J. Peng, S.Q. Zhang, S.-G. Zhou, Phys. Rev. C **73** (2006) 037303.
- [26] S.Y. Wang, S.Q. Zhang, B. Qi, J. Meng, Phys. Rev. C **75** (2007) 024309.
- [27] G. Rainovski *et. al.*, Phys. Rev. C **68** (2003) 024318.
- [28] P. Joshi *et. al.*, Phys. Lett. B **595** (2004) 135.
- [29] J. Peng, J. Meng, S.Q. Zhang, Phys. Rev. C **68** (2003) 044324.
- [30] I. Hamamoto, Int. J. Mod. Phys. E **20** (2011) 373.
- [31] T. Koike, K. Starosta, I. Hamamoto, Phys. Rev. Lett. **17** (2004) 172502.
- [32] A. J. Simons *et. al.*, J. Phys. G: Nucl. Part. Phys. **31** (2005) 541.